MNRAS **000**, 1–15 (2020) Preprint 10 January 2020 Compiled using MNRAS LATEX style file v3.0

A search for Centaurus A-like features in the spectra of *Fermi*-LAT detected radio galaxies

Cameron B. Rulten,[1]★ Anthony M. Brown,[1] and Paula M. Chadwick,[1]
[1] *Centre for Advanced Instrumentation, Department of Physics, University of Durham, South Road, Durham, DH1 3LE, United Kingdom*

Accepted 2020 January 3. Received 2019 December 16; in original form 2019 September 6

ABSTRACT

Motivated by the detection of a hardening in the γ-ray spectrum of the radio galaxy Centaurus A, we have analysed ∼10 years of *Fermi*-LAT observations of 26 radio galaxies to search for similar spectral features. We find that the majority of the radio galaxies' γ-ray spectral energy distributions are best fitted with a simple power-law model, and no spectral hardening similar to that found in Centaurus A was detected. We show that, had there been any such spectral features present in our sample of radio galaxies, they would have been seen, but note that 7 of the radio galaxies (3C 111, 3C 120, 3C 264, IC 4516, NGC 1218, NGC 2892 and PKS 0625-35) show evidence for flux variability on 6-month timescales, which makes the detection of any steady spectral features difficult. We find a strong positive correlation (r = 0.9) between the core radio power at 5 GHz and the γ-ray luminosity and, using a simple extrapolation to TeV energies, we expect around half of the radio galaxies studied will be detectable with the forthcoming Cherenkov Telescope Array.

Key words: gamma-rays: galaxies – galaxies: active – radiation mechanisms: non-thermal

1 INTRODUCTION

In the recently released *Fermi*-LAT 4FGL 8–year point source catalog (The Fermi-LAT collaboration 2019), nearly 70% of the objects are associated with a known astrophysical object. Of these associated sources, the majority are classified as blazars: either of type BL Lac (∼22%) or blazar, classification unknown (∼23%). Additionally, Flat Spectrum Radio Quasars (FSRQs) account for ∼13% of the associated point sources in the 4FGL. Less than 1% of all 4FGL sources are associated with radio galaxies.

According to the unified model of active galactic nuclei (AGN) (Urry & Padovani 1995), radio galaxies are radio–loud AGN that have jets beamed at large inclination angles with respect to the observer's line of sight, and are therefore sometimes termed misaligned blazars. Unlike blazars, therefore, the non-thermal radiation emitted by radio galaxies is only modestly beamed (Rieger 2017). Thus radio galaxies are very interesting targets because any detected γ-ray signal from these AGN is not dominated by the highly beamed jet emission, meaning it might be possible to disentangle jet and core emission or even to detect other potential sources of γ-ray emission.

The nearby, well-studied and (on *Fermi*-LAT timescales) non-variable object Centaurus A (Cen A) is an obvious target to search for emission which does not originate in the jet. A study of Brown et al. (2017) revealed evidence for a new population of energetic particles near Cen A's core. This evidence was manifested as a statistically significant ($> 5\sigma$) hardening in the Fermi-LAT γ-ray spectrum, with the spectral index changing from $\Gamma = 2.73 \pm 0.02$ to $\Gamma = 2.29 \pm 0.07$ at a break energy of 2.6 ± 0.3 GeV.

The study of Cen A was motivated by a possible mechanism for the origin of the most energetic cosmic rays (CRs) in AGN. Such CRs extend to energies beyond $> 10^{20}$eV, making it difficult to explain the energy spectrum if CRs represent an accelerated thermal population. To solve this problem it might be possible to use dark matter (DM) annihilations as a source of non-thermal particles that can be further accelerated in astrophysical shocks. These shock–accelerated particles should produce a power-law spectrum for all energies, and the DM annihilation should produce a spectrum with a cut-off at the DM particle mass. The combination of these two effects should result in a characteristic spectrum (Lacroix et al. 2014).

The lack of variability in Cen A's emission ruled out the possibility of jet-induced leptonic processes being responsible for the spectral feature and it was found that the γ-ray spectrum of Cen A was compatible with a very large

★ E-mail: cameron.b.rulten@durham.ac.uk

localized enhancement (i.e. a spike) in the DM halo profile (Brown et al. 2017). However, it was noted that a population of unresolved millisecond pulsars or another population of energetic particles could also be responsible for the emission above 2.6 GeV. Recent results from the H.E.S.S. telescopes have resolved the emission above 100 GeV, and suggest that the highest-energy emission from Cen A comes from a small, inner jet close to Cen A's core (Sanchez et al. (2018); H. E. S. S. Collaboration et al. (2018b)), which could well be the source of the population of energetic particles postulated in Brown et al. (2017).

The discovery of a spectral hardening of Cen A's γ-ray spectrum provides the motivation to look at other radio galaxies detected with *Fermi*-LAT in order to search for similar spectral features. This work describes our analysis of a selection of such radio galaxies. In Section 2 we highlight the *Fermi*-LAT observations used, our radio galaxy selection criteria, and the data analysis methods employed. In Section 3 we focus on the results of our *Fermi*-LAT analysis before discussing possible interpretations of our findings in Section 4.

2 *Fermi*-LAT OBSERVATIONS AND DATA ANALYSIS

The Large Area Telescope [LAT; Atwood et al. (2009)] aboard the NASA *Fermi* γ-ray Space Telescope is a wide–field pair conversion telescope sensitive to γ-rays over the approximate energy range 30 MeV $\leqslant$ E $\leqslant$ 300 GeV. The *Fermi*-LAT was launched from the Kennedy Space Center on June 11, 2008 and started conducting science operations on 11th August 2008; it has thus recently celebrated 11 years of near uninterrupted service. The great majority of data taken by *Fermi*-LAT during this time has been in all-sky-survey mode. This observing mode scans the entire sky every $\sim$180 minutes and has produced the deepest extragalactic scan ever at γ-ray energies.

2.1 Radio galaxy selection

The 26 radio galaxies selected and listed in Table 1 are those identified and categorized as radio galaxies in the *Fermi*-LAT 4FGL catalog (The Fermi-LAT collaboration 2019), excluding four well–studied, nearby radio galaxies: M 87, the Perseus cluster galaxies NGC 1275 and IC 310, all of which have been found to exhibit significant flux variability at γ-ray energies ((Ait Benkhali et al. 2019; Brown & Adams 2011; Aleksić et al. 2014) respectively) and Cen A (Brown et al. 2017). We have included PKS 0625-35 in the list of selected radio galaxies; however, as discussed in a recent paper (H. E. S. S. Collaboration et al. 2018a), there is evidence to suggest that this galaxy could be a BL Lac object and thus its classification as a "misaligned blazar" may need to be reconsidered. The majority of the radio galaxies in our study are classified as having a Fanaroff-Riley type I (FR I) morphology (Fanaroff & Riley 1974); there are 6 Fanaroff-Riley type 2 (FR II) galaxies, and one compact radio galaxy (FR 0).

Our selection does not, of course, represent a complete list of radio galaxies detected above 20 MeV, as there is always the possibility that some of the 1500+ unassociated sources in the 4FGL catalog may be radio galaxies.

2.2 Data analysis

Roughly 10 years worth of *Fermi*-LAT data were used for each target. The exact exposure spans MJD 54682.65527778 through to and including MJD 58362.0, which is equivalent to 317895388 *Fermi*-LAT seconds, 3679.34 *Fermi*-LAT days or 10.08 *Fermi*-LAT years. We consider photons with energies between $0.1 - 300$ GeV within a 15° circular region of interest (ROI) centred on each radio galaxy target. These photons were obtained from *Fermi*-LAT sky-survey observations in accordance with the PASS8 data analysis criteria. The *Fermi*-LAT recommended quality cuts were used, including a zenith angle cut of 90° (to reduce γ-ray contamination originating from the Earth's limb), `(DATA_QUAL>0)&&(LAT_CONFIG==1)` and `abs(rock_angle)` < 52.

We used the open–source `Python` package `Fermipy` (Wood et al. 2017) to facilitate analysis of *Fermi*-LAT data with the *Fermi*-LAT `Fermitools` (v1.0.1). The analysis used the `P8R3_SOURCE_V2` instrument response function and adopted the binned maximum-likelihood method (Mattox et al. 1996). To estimate the background, we included sources within the region of interest (ROI) listed in the 4FGL catalog (The Fermi-LAT collaboration 2019) along with the recommended Galactic (`gll_iem_v07.fits`) and isotropic diffuse (`iso_P8R3_SOURCE_V2_v1.txt`) templates provided with the `Fermitools`.

Since our study considered 10 years of *Fermi*-LAT observations, we must search for additional point sources of γ-rays not accounted for by the 8-year integrated catalogue of the 4FGL. To do this, we used the `find_sources` algorithm in `Fermipy` to construct a significance map centred on each radio galaxy candidate[1]. This TS map was used to identify additional point sources of γ-rays, with TS $\geqslant 25$, that were not accounted for in our initial model. These new point sources were modelled using a power-law fixed at the location $(\alpha_{J2000}, \beta_{J2000})$ of the peak excess, and a final likelihood fit was performed with the normalisation and spectral index of the new point sources free to vary.

3 RESULTS

Once all sources of γ-rays were accounted for in our data, we conducted temporal and spectral studies for all 26 radio galaxies considered in our research. For each, we produced a spectral energy distribution (SED); these are shown in Figures 1 and 2. The SED flux points are generated using a separate likelihood analysis for each equally–spaced logarithmic energy bin. For each target we initially used 8 bins per decade, but then rebinned the flux data into a binning scheme of 2 bins per decade. Each spectral bin requires a statistical significance above background as defined by the

[1] The significance map was constructed assuming a point source with an E^{-2} spectrum.

Fermi-LAT name	Assoc. name	l (deg.)	b (deg.)	z	Morphology	Variability index	σ ($\sqrt{TS}$)
4FGL J0322.6-3712e	Fornax A	240.16	-56.68	0.0059	FR I	36.5	16.99
4FGL J0057.7+3023	NGC 315	124.56	-32.49	0.0164	FR II	21.0	9.03
4FGL J0708.9+4839	NGC 2329	168.57	22.79	0.0197	-	4.0	7.23
4FGL J0334.3+3920	4C +39.12	154.16	-13.43	0.0203	FR 0	20.1	8.81
4FGL J1144.9+1937	3C 264†	235.72	+73.03	0.0216	FR I	66.5	11.38
4FGL J0931.9+6737	NGC 2892	145.14	+39.87	0.0226	-	45.9	16.76
4FGL J1630.6+8234	NGC 6251	115.76	+31.19	0.0239	FR I	39.7	38.33
4FGL J0009.7-3217	IC 1531	2.39	-32.27	0.0256	-	38.1	7.46
4FGL J2156.0-6942	PKS 2153-69	321.31	-40.6	0.0280	-	22.2	8.80
4FGL J0308.4+0407	NGC 1218	174.85	-44.51	0.0288	FR I	49.1	20.15
4FGL J1449.5+2746	B2 1447+27	41.25	63.87	0.0308	-	7.4	5.30
4FGL J0433.0+0522	3C 120	190.37	-27.39	0.0336	FR I	306.8	24.56
4FGL J0519.6-4544	Pictor A	251.59	-34.63	0.0340	FR II	10.7	10.59
4FGL J0758.7+3746	NGC 2484	182.67	+28.82	0.0408	FR I	10.3	4.80
4FGL J1454.1+1622	IC 4516	223.59	+16.35	0.0452	FR II	73.3	13.71
4FGL J0418.2+3807	3C 111	161.67	-08.81	0.0485	FR II	89.9	19.07
4FGL J2341.8-2917	PKS 2338-295	355.36	-29.31	0.0523	-	38.1	6.63
4FGL J1516.5+0015	PKS 1514+00	1.38	45.98	0.0526	FR II	17.9	8.73
4FGL J0627.0-3529	PKS 0625-35 †	243.45	-19.96	0.0562	FR I	42.7	33.65
4FGL J1306.3+1113	TXS 1303+114	316.05	73.71	0.0857	FR I	7.6	4.95
4FGL J1518.6+0614	TXS 1516+064	8.86	49.25	0.1021	FR I	6.3	6.49
4FGL J1843.4-4835	PKS 1839-48	347.17	-18.72	0.1112	FR I	15.0	6.15
4FGL J1306.7-2148	PKS 1304-215	307.62	40.92	0.1260	-	22.8	11.85
4FGL J2302.8-1841	PKS 2300-18	45.89	-63.71	0.1289	-	18.0	9.44
4FGL J1443.1+5201	3C 303	90.52	+57.50	0.1412	FR II	22.2	7.38
4FGL J2326.9-0201	PKS 2324-02	351.72	-02.03	0.1880	-	35.8	6.32

Table 1. Details of the radio galaxies analyzed in this study including their *Fermi*-LAT variability index and detection significance (obtained in this work). The radio galaxies were selected using the *Fermi*-LAT 4FGL catalog and are ordered by increasing redshift (z). A variability index > 39.7 indicates a $< 1\%$ chance of being a steady source. The two TeV-detected radio galaxies are highlighted with a †.

test statistic, TS [2], such that $\sqrt{\mathrm{TS}} \geqslant 2\sigma$, and a minimum number of γ-ray photons above background of $\gamma \geqslant 2$; otherwise a 95% confidence–level upper limit is calculated. For each SED we also calculate and show the 1σ uncertainty band. For each radio galaxy we initially only considered the spectral model given in the 4FGL catalogue as a description of the high-energy γ-ray emission. In the NGC 1218 SED (Figure 2) we see some tension between a power-law model description and the highest energy bin upper limit. As a result we also considered a log-parabola model for NGC 1218, and find that with a test statistic value of 235 between the log-parabola and power-law models, the fit significantly improves and hence we discard the initial power-law model.

As can be seen in Figures 1, 2, 3 and 4, the 10-year SEDs produced do not share the spectral features which were seen in Cen A (Brown et al. 2017). Instead, the majority of radio galaxy SEDs are best fitted with a simple power-law model. The exceptions are 3C 120, NGC 1218, NGC 6251 and PKS 2152-69, which are best fitted with a log-parabola model. We also note that NGC 2484, PKS 1839-48, TXS 1303+114 and TXS 1516+064 have only 2 statistically significant spectral flux bins above background; unsurprisingly, these targets are amongst those with the lowest detection significances within this analysis. Both NGC 2484 and TXS 1303+114 fall just below the accepted 5σ significance threshold in this 10-year dataset, and in both cases, their SEDs lack sufficient statistics across the full energy band to produce a reliable power-law fit.

In most cases we detect no significant γ-ray excess above 30 GeV. The exceptions to this are 3C 264, 4C +39.12, B2 1447+27, Fornax A, NGC 1218, NGC 2329 and PKS 0625-35. Two of these are detected at TeV energies: PKS 0625-35 (H. E. S. S. Collaboration et al. 2018a) and 3C 264 (Mukherjee 2018). Apart from Fornax A, these radio galaxies all exhibit fairly hard spectra over the energy band considered in this analysis. In addition, 3C 264 and 4C +39.21 share very similar SED characteristics across the *Fermi*-LAT energy band. Intriguingly, no significant γ-ray excess above background is detected for either of these two radio galaxies at energies below 1 GeV. Above 1 GeV their flux brightness is similar and their spectral indices are hard (0.1 and 0.14 respectively in $\mathrm{E}^2\mathrm{dNdE}$ units), resulting in a significant γ-ray excess up to energies of 100 GeV. Given 3C 264 was recently detected by VERITAS at TeV energies (Mukherjee 2018), perhaps there is potential for detecting 4C +39.12 at TeV energies too. If detected, it would be the lowest luminosity radio galaxy yet seen at TeV energies apart from IC 310, a peculiar galaxy with somewhat uncertain classification (Graham et al. 2019).

In addition to this spectral investigation, we also investigated the temporal characteristics by producing lightcurves for each radio galaxy studied. Relative to blazars, radio galaxies are weak γ-ray emitting sources and at the energies we are considering, *Fermi*-LAT does not have the sensitivity performance to detect enough γ-ray photons for

[2] Defined as twice the difference between the log-likelihoods of two different models, $2logL - logL_0$, where L and L_0 are defined as the likelihoods of individual model fits (Mattox et al. 1996).

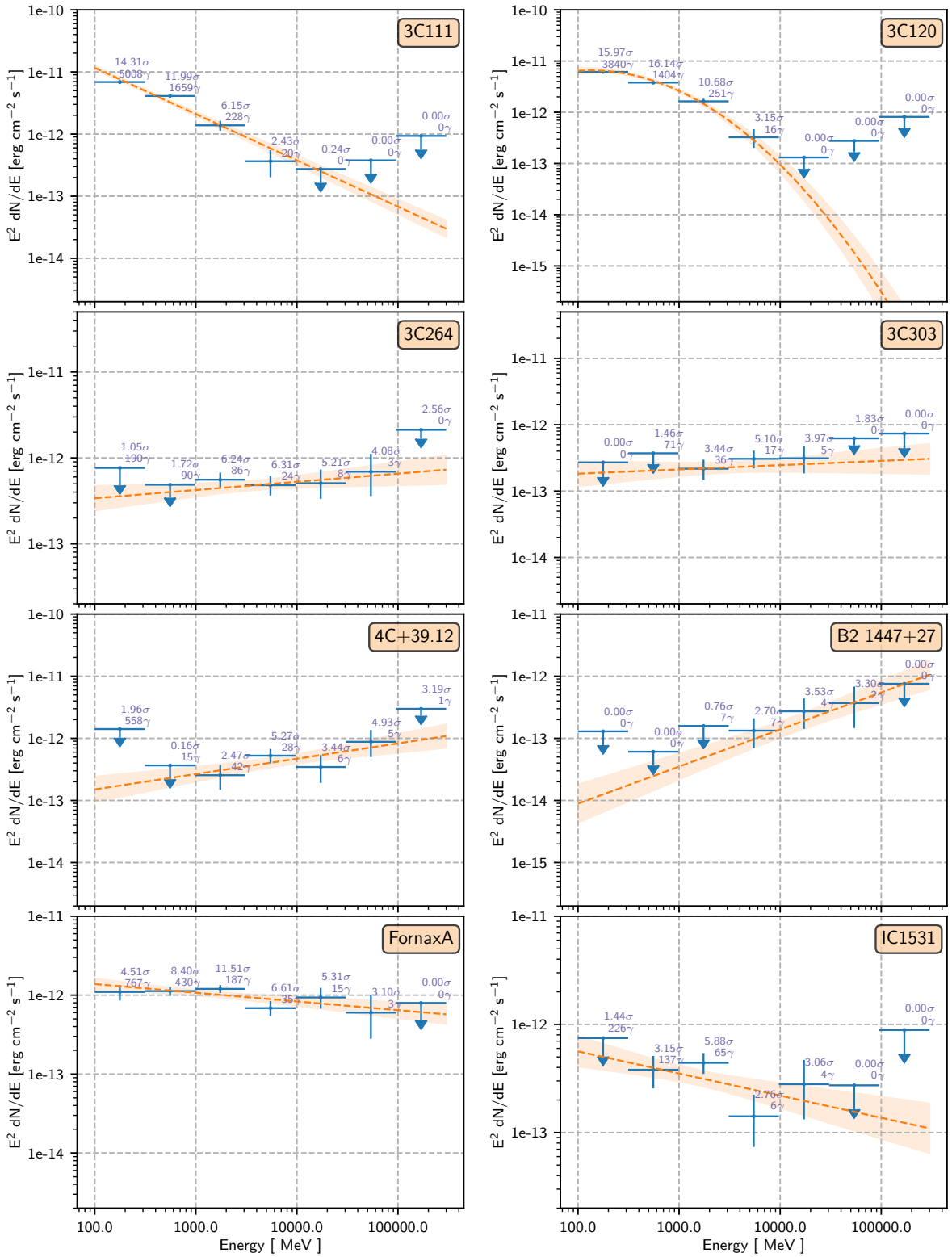

Figure 1. Spectral energy distributions obtained for the radio galaxies: 3C 311, 3C 120, 3C 264, 3C 303, 4C +39.12, B2 1447+27, Fornax A and IC 1531. Apart from 3C 120, all the radio galaxy SEDs in this subset are best-fitted with a simple power-law model. The binning scheme is 2 bins per decade and a 95% confidence–level upper limit is shown for bins where $\sqrt{\mathrm{TS}} < 2\sigma$ and the number of γ-ray photons above background in each bin is $\gamma < 2$.

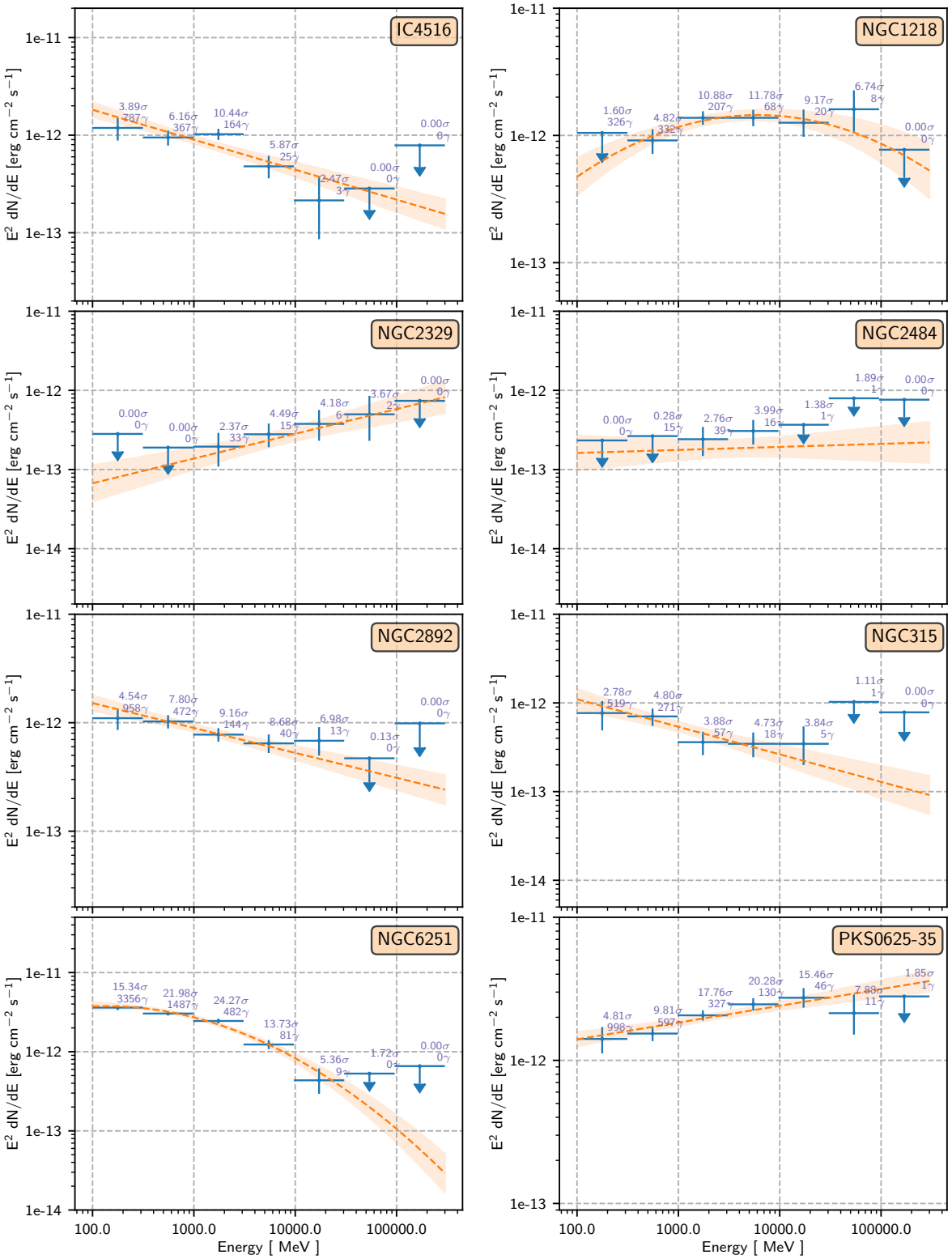

Figure 2. Spectral energy distributions obtained for the radio galaxies IC 4516, NGC 1218, NGC 2329, NGC 2484, NGC 2892, NGC 315, NGC 6251 and PKS 0625-35. Apart from NGC 1218 and NGC 6251, all the radio galaxy SEDs in this subset are best-fitted with a simple power-law model. The binning scheme is 2 bins per decade and a 95% confidence–level upper limit is shown for bins where $\sqrt{\mathrm{TS}} < 2\sigma$ and the number of γ-ray photons above background in each bin is $\gamma < 2$.

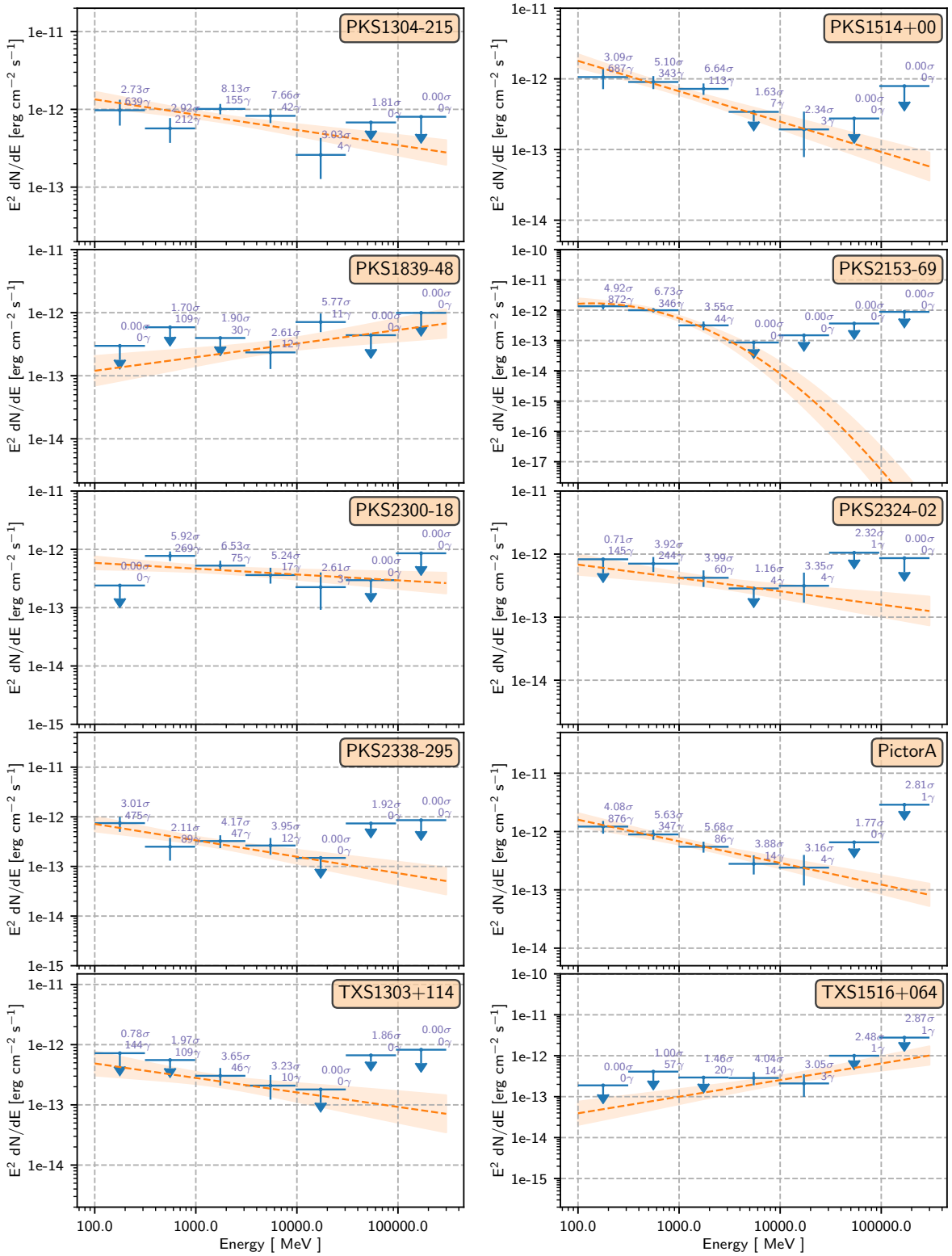

Figure 3. Spectral energy distributions obtained for the radio galaxies PKS 1304-215, PKS 1514+00, PKS 1839-48, PKS 2153-69, PKS 2300-18, PKS 2324-2, PKS 2338-295, Pictor A, TXS 1303+114 and TXS 1516+064. Apart from PKS 2153-69, all the radio galaxy SEDs in this subset are best-fitted with a simple power-law model. The binning scheme is 2 bins per decade and a 95% confidence–level upper limit is shown for bins where $\sqrt{\mathrm{TS}} < 2\sigma$ and the number of γ-ray photons above background in each bin is $\gamma < 2$.

Fermi-LAT name	Assoc. name	N_0 (cm^{-2} s^{-1} MeV^{-1})	Index (Γ)	E_0 (MeV)	E_{pivot} (MeV)
4FGL J0418.2+3807	3C 111	$(7.39 \pm 0.46) \times 10^{-12}$	-2.75 ± 0.05	532.8	300.0
4FGL J1144.9+1937	3C 264	$(2.84 \pm 0.39) \times 10^{-14}$	-1.90 ± 0.10	3216.4	3601.2
4FGL J1443.1+5201	3C 303	$(1.22 \pm 0.24) \times 10^{-14}$	-1.94 ± 0.14	3426.4	3250.7
4FGL J0334.3+3920	4C +39.12	$(7.90 \pm 1.48) \times 10^{-15}$	-1.75 ± 0.13	5679.6	6777.7
4FGL J1449.5+2746	B2 1447+27	$(7.23 \pm 2.49) \times 10^{-16}$	-1.40 ± 0.20	11380.8	13137.0
4FGL J0322.6-3712e	Fornax A	$(2.02 \pm 0.15) \times 10^{-13}$	-2.11 ± 0.06	1762.5	1396.5
4FGL J0009.7-3217	IC 1531	$(6.88 \pm 1.22) \times 10^{-14}$	-2.2 ± 0.13	1692.2	1440.7
4FGL J1454.1+1622	IC 4516	$(6.76 \pm 0.63) \times 10^{-13}$	-2.31 ± 0.07	922.3	1073.6
4FGL J0708.9+4839	NGC 2329	$(6.32 \pm 1.52) \times 10^{-15}$	-1.69 ± 0.15	4693.8	7416.6
4FGL J0758.7+3746	NGC 2484	$(9.88 \pm 2.82) \times 10^{-15}$	-1.96 ± 0.17	3421.0	3346.8
4FGL J0931.9+6737	NGC 2892	$(2.40 \pm 0.19) \times 10^{-13}$	-2.23 ± 0.06	1459.5	1205.1
4FGL J0057.7+3023	NGC 315	$(2.56 \pm 0.35) \times 10^{-13}$	-2.31 ± 0.11	1124.0	1158.9
4FGL J0627.0-3529	PKS 0625-35	$(2.32 \pm 0.11) \times 10^{-13}$	-1.88 ± 0.04	2337.5	2215.6
4FGL J1306.7-2148	PKS 1304-215	$(9.91 \pm 1.16) \times 10^{-14}$	-2.20 ± 0.08	2151.2	1640.5
4FGL J1516.5+0015	PKS 1514+00	$(8.55 \pm 1.13) \times 10^{-13}$	-2.43 ± 0.10	744.0	852.7
4FGL J1843.4-4835	PKS 1839-48	$(1.09 \pm 0.27) \times 10^{-14}$	-1.78 ± 0.16	3893.3	6115.0
4FGL J2302.8-1841	PKS 2300-18	$(8.58 \pm 1.22) \times 10^{-14}$	-2.10 ± 0.09	1788.0	1530.9
4FGL J2341.8-2917	PKS 2338-295	$(7.56 \pm 1.47) \times 10^{-14}$	-2.33 ± 0.15	1548.7	1157.3
4FGL J0519.6-4544	Pictor A	$(1.72 \pm 0.23) \times 10^{-13}$	-2.37 ± 0.10	1462.0	1397.7
4FGL J2326.9-0201	PKS 2324-02	$(1.70 \pm 0.36) \times 10^{-13}$	-2.21 ± 0.13	1215.0	2048.4
4FGL J1306.3+1113	TXS 1303+114	$(7.06 \pm 2.16) \times 10^{-15}$	-2.24 ± 0.19	4187.4	1604.0
4FGL J1518.6+0614	TXS 1516+064	$(3.75 \pm 1.11) \times 10^{-15}$	-1.59 ± 0.19	5831.5	10929.7

Table 2. Details of the power-law models best fitted to the radio galaxy SEDs.

.

Fermi-LAT name	Assoc. name	N_0 (cm^{-2} s^{-1} MeV^{-1})	Index (α)	Curvature (β)	E_0 (MeV)	E_{pivot} (MeV)
4FGL J0433.0+0522	3C 120	$(14.8 \pm 0.86) \times 10^{-12}$	2.55 ± 0.07	0.23 ± 0.05	445.8	366.8
4FGL J0308.4+0407	NGC 1218	$(7.27 \pm 0.78) \times 10^{-13}$	1.76 ± 0.10	0.07 ± 0.03	1000.0	2518.8
4FGL J1630.6+8234	NGC 6251	$(4.28 \pm 0.17) \times 10^{-12}$	2.26 ± 0.04	0.08 ± 0.02	667.8	479.9
4FGL J2156.0-6942	PKS2153-69	$(5.68 \pm 0.91) \times 10^{-12}$	2.57 ± 0.23	0.29 ± 0.18	368.8	295.5

Table 3. Details of the log-parabola model best fitted to the radio galaxy SEDs.

.

a well-sampled lightcurve at timescales under 6 months. Therefore we constructed lightcurves using 20 time bins with each bin comprising 180 days of *Fermi*-LAT data covering the full 10 year observation period.

The lightcurves were produced using a binned likelihood approach where the normalisation value for the radio galaxy of interest, all sources within 1 degree of the radio galaxy and the diffuse background were kept free to vary. For each time bin a flux is calculated over the full energy range 100 MeV $\leqslant$ E $\leqslant$ 300 GeV. A variability index (see Table 1) was calculated for each radio galaxy using the method described in Nolan et al. (2012) which is a simple Likelihood Ratio test between the null hypothesis (a constant source) and the alternative hypothesis (variable source). If the null hypothesis is correct, then in accordance with this method, the variability index is distributed as χ^2 with 19 degrees of freedom. Thus any variability index above 39.7 indicates evidence for variability at the $\geqslant 3\sigma$ level. We find statistical evidence of flux variability on 6 month timescales for seven of the 26 radio galaxies analysed: 3C 111, 3C 120, 3C 264, IC 4516, NGC 1218, NGC 2892 and PKS 0625-35.

While fixed-time-width binning schemes, like that used in our temporal analysis are widely used within the field, there is merit in exploring a Bayesian Block binning scheme for the radio galaxies we identify here as variable. Such an analysis will aid the comparison of spectra obtained for flaring and non-flaring states and may enable us to uncover any Cen A-like spectral components potentially camouflaged by variable components. Such an analysis will be the subject of a future publication.

4 INTERPRETATION

Our analysis shows that the SEDs of the radio galaxies studied do not exhibit any spectral features to warrant fitting any extra spectral components. Although no firm conclusions can be drawn without a full multi-wavelength analysis on a source by source basis, it does appear as though the γ-ray emission found in the *Fermi*-LAT categorised radio galaxies at energies 10 MeV $\leqslant$ E $\leqslant$ 300 GeV is dominated by jet particle acceleration and/or jet interaction. This is particularly the case for the 7 objects which display evidence for variability; such variability not only suggests a jet origin for the emission, but renders it difficult to detect any steady spectral features which may exist (Graham et al. 2019). For example, in blazars we know that the variable emission we detect is dominated by emission processes in their ultra-relativistic jets. TeV emission from blazars due to VLBI knots is seen in jets with variability timescales typically lasting minutes to hours during flaring periods. In the case of two radio galaxies, M 87 and IC 310, the variability timescales detected are much shorter than the light crossing time of the black hole horizon, which implies the γ-ray

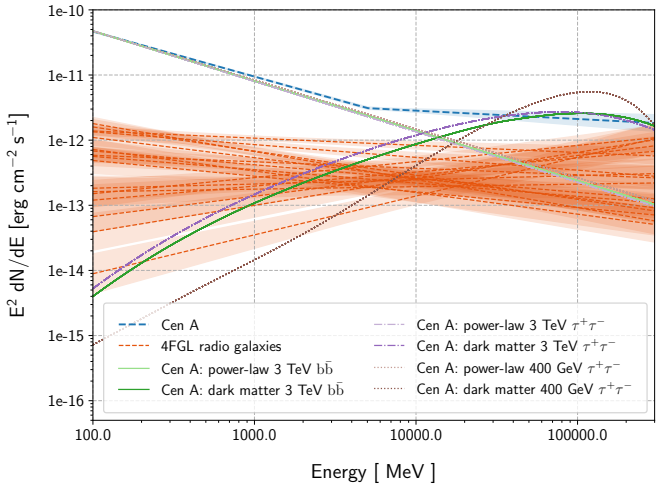

Figure 4. Shown here is a comparison of the SED shapes obtained for Cen A (blue dashed line) versus the best fitted power-law spectral shapes for the non-variable 4FGL radio galaxies analysed in this work (orange dashed lines). Also shown is the 1 sigma confidence bands obtained for Cen A (blue band) and the 4FGL radio galaxies (orange bands). It is clear that if there were any Cen A-like spectral features present in the sample of radio galaxies analysed, we would have seen them. We have also overlaid the power-law and DM models (see legend) used to describe the total Cen A emission (Brown et al. 2017) for the given DM particle mass and annihilation channel. Assuming the supermassive black holes of the 4FGL radio galaxies are of a similar mass scale to that of Cen A's, which implies that the total mass of DM in the 4FGL radio galaxies is similar to that of Cen A, we see no evidence of spectral hardening in the *Fermi*-LAT energy band to warrant consideration of DM scenarios.

emission must be coming from a compact region (Giannios et al. 2009).

It is immediately obvious from Figure 4 that if there were any spectral features similar to that seen in Cen A, they would have been detected. However, as the supermassive black hole masses for the radio galaxies are not known and the mass of the DM spike expected around the central SMBH is related to the mass of the SMBH, detailed modelling of any DM signal one might expect from these radio galaxies and how that compares to the Cen A DM model fitted by Brown et al. (2017) is not possible; we can simply say that there is no such component at a similar level to that observed in Cen A. The observational evidence from *Fermi*-LAT and H.E.S.S. suggests that whatever is happening in Cen A is unusual, or perhaps spectral features are simply easier to detect due to the object's proximity. The lack of evidence for variability in the γ-ray emission from Cen A means theorists are able to postulate scenarios where the γ-ray emission arises from larger scales i.e. not a compact emitting region. Such scenarios could include contributions from undetected millisecond pulsars or dark matter (Brown et al. 2017) or hadronic processes such as the interaction of energetic protons with ambient matter (proton-proton interactions) (Sahakyan et al. 2013) or the inverse Compton upscattering of photons on kiloparsec scales (Hardcastle & Croston 2011) or host galaxy starlight (Stawarz et al. 2003). These scenarios are largely degenerate and the only way to distinguish these models from one another is to accumulate more and better quality radio and ground-based TeV observations of radio galaxies.

Six of the radio galaxies studied, 3C 264, 4C +39.12, B2 1447+27, NGC 1218, NGC 2329 and PKS 0625-35, have particularly hard spectra and emission above 30 GeV. Furthermore, two of these objects, 3C 264 and 4C +39.21, show no significant excess below 1 GeV. It is possible that the hard spectra displayed by these objects are an indication that the peak of the inverse Compton emission is located in the *Fermi*-LAT energy regime. This would be surprising, as radio galaxies do not have the strong Doppler-boosting normally required to produce such a high-frequency peak in their SED. Multi-wavelength observations would be required to confirm if this is the case.

In the case of Cen A, the H.E.S.S. observations were really important in the identification of a statistically significant spectral hardening. Thus, with the construction of new ground-based instruments like CTA about to begin, we need to look for any hints of correlation across multiwavelength data to try and pinpoint the best radio galaxy candidates for observation with IACTs, which ultimately will help us to better understand any such spectral upturns and if they are a common occurrence in these galaxies. We therefore used our analysis results to search for correlations between a number of different characteristic properties and the γ-ray emission from these radio galaxies. Figures 5 and 6 show the results of our correlation studies using data from publicly accessible radio and optical catalogues.

In Figure 5 the left panel shows the radio luminosity calculated using the *total* 5 GHz radio flux density versus the γ-ray luminosity calculated using the integrated fluxes estimated in this work, assuming a concordance cosmology with $H_0 = 71$ km s^{-1} Mpc^{-1}, $\Omega_M = 0.27$, $\Omega_\Lambda = 0.73$ and $T_{CMB} = 2.725$ K. Where no 5 GHz flux densities were available we used the 4.8 GHz flux density measurement. We find a strong positive correlation between the radio and γ-ray luminosity, with the correlation coefficient r = 0.8. The right panel shows the absolute magnitude of the visual optical band calculated using extinction corrected V filter data versus the γ-ray luminosity, calculated using the integrated fluxes estimated in this work. Where no V filter data were available we used B filter data. We find a weak positive correlation (r = 0.4) between the absolute magnitude of these radio galaxies versus their γ-ray luminosity. We also highlight and annotate the power-law modelled TeV-detected radio galaxies using blue star markers, and we see no clustering of these particular sources.

The left panel of Figure 6 shows the radio power of the *core* at 5 GHz frequencies versus the γ-ray luminosity calculated using the integrated fluxes estimated in this work. Where no 5 GHz data were available we used the 4.8 GHz radio flux densities to estimate the core radio power. We find a strong positive correlation between the core radio power at 5 GHz frequencies versus the γ-ray luminosity, with the correlation coefficient r = 0.9. The right panel shows the γ-ray luminosity calculated using the integrated fluxes estimated in this work versus the radio core dominance parameter calculated using the method highlighted in Fan & Zhang (2003). The core dominance parameter suffers from a number of different systematic uncertainties (Abdo et al. 2010), and as reported elsewhere (Angioni et al. 2019) we

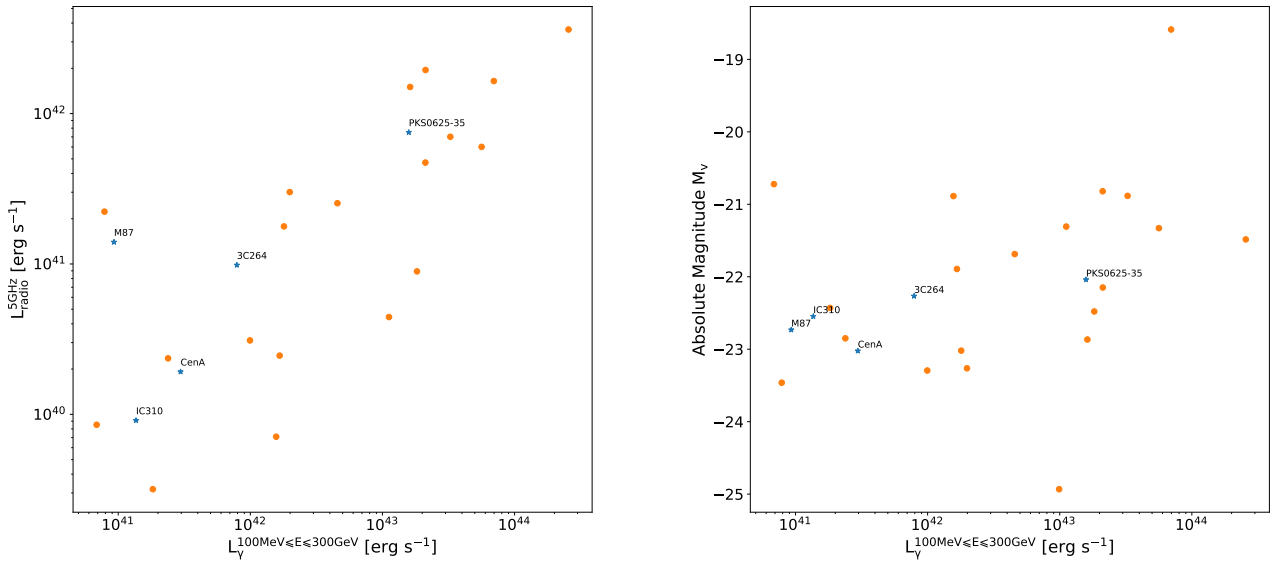

Figure 5. The left panel shows the radio luminosity calculated using the total 5 GHz (where not available we used 4.8 GHz) radio flux density available in publicly accessible radio catalogues versus the γ-ray luminosity calculated using the integrated fluxes estimated in this work. We find a strong positive correlation between the radio and γ-ray luminosity. The right panel shows the absolute magnitude for the visual optical band primarily using extinction corrected V filter data (where not available we used B filter data) versus the γ-ray luminosity calculated using the integrated fluxes estimated in this work. We calculated the absolute magnitudes using photometric data available in NED and Simbad (Wenger et al. 2000), except for PKS 0625-35 (Massardi et al. 2008). We find a weak correlation between the optical brightness of these radio galaxies versus their γ-ray luminosity. The TeV-detected radio galaxies are annotated and highlighted using blue star markers, and we see no clustering of these particular sources. The Cen A γ-ray luminosity was calculated assuming a power-law model and not the broken power-law model from Brown et al. (2017).

find no correlation between the γ-ray luminosity and the radio core dominance parameter, with correlation coefficient r = −0.3. Again we highlight and annotate the TeV-detected radio galaxies using blue star markers, and we see no clustering of these particular sources.

Finally, in the context of potentially correlated γ-ray and radio flux, we also investigated the possibility of extended γ-ray emission associated with the kiloparsec scale jet of the radio galaxies. For each radio galaxy we produced a skymap as seen in Figures 7 and 9. Each of these show the significance ($\sqrt{\mathrm{TS}}$) for an approximate 2 degree region centred on the radio galaxy target (indicated with a green x). Significance values greater than 5 σ are enclosed within the solid dark-orange contour line, and values greater than 15 σ are enclosed within the solid light-orange contour line. We note that there is apparent evidence for extended emission coming from the direction of 3C 111. However, on closer inspection this extension is likely an artefact of nearby ($< 1.5^{\circ}$) point sources just below the detection threshold.

As discussed above, radio galaxies are very interesting targets for a host of reasons. With the forthcoming next-generation ground-based γ-ray observatory the Cherenkov Telescope Array (CTA) (CTA Consortium & Ong (2019); Angioni et al. (2017)), it is hoped that a larger sample of radio galaxies emitting radiation at very-high-energies will be gathered. Figure 10 shows the *Fermi*-LAT 4FGL radio galaxy fluxes extrapolated to 100 TeV for both CTA-South (left panel) and CTA-North (right panel) respectively. The *Fermi*-LAT detected fluxes were extrapolated assuming no breaks or features in the spectra from the GeV to TeV energy regime. CTA's ten times better sensitivity over the core energies compared to existing ground-based instruments should enable the detection of approximately 13 of the radio galaxies analysed in this work, assuming a 50 hour observation using the CTA-North and CTA-South arrays respectively. In practice, CTA has the potential to detect a larger number, as there are bound to be variable radio galaxies that will be seen with CTA during flaring periods.

5 CONCLUSIONS

The discovery of a distinctive break in the power-law spectrum of Cen A posed many questions concerning the origin and mechanisms behind the spectral hardening. We therefore analysed 26 other *Fermi*-LAT-detected radio galaxies to see whether any other "similar" objects to Cen A exhibit breaks and spectral hardening. This work has found no evidence for spectral hardening over a 10-year-averaged spectrum calculated for each radio galaxy. Had there been such a spectral feature in these objects, it would have been apparent in the data we analysed. This suggests that either Cen A is unique among radio galaxies, or that any break occurs outside *Fermi*-LAT's energy range. We also noted that a number of the galaxies analysed show variability on the 6-month timescale, which strongly suggests a jet origin for the

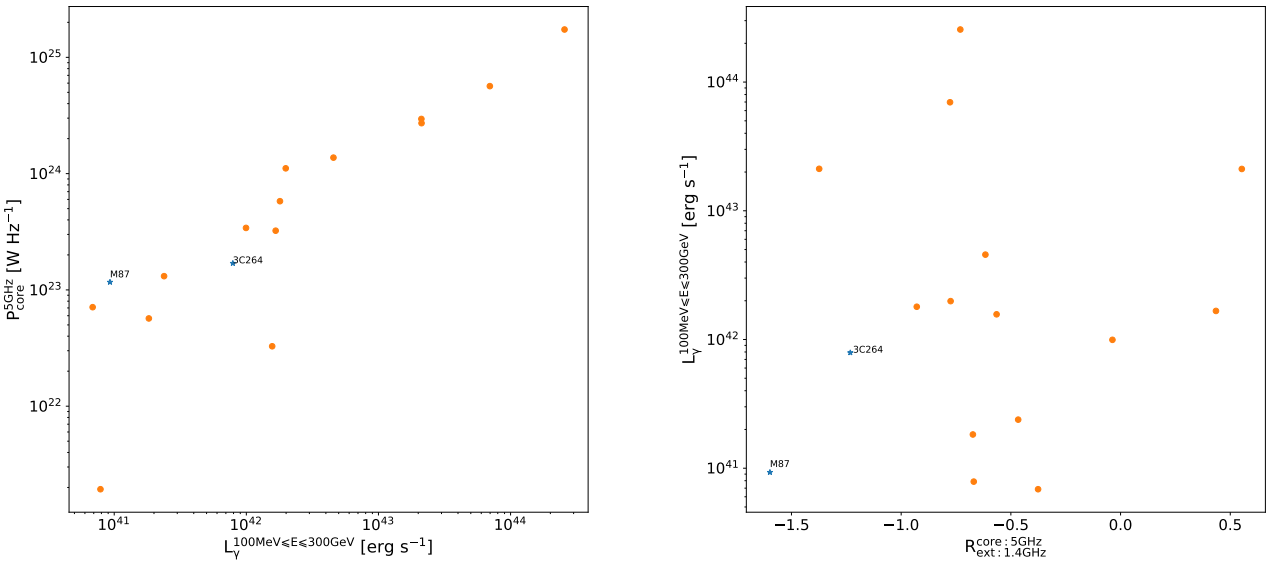

Figure 6. The left panel shows the radio core power calculated using the core 5 GHz (except for PKS 2324-02 we used 4.8 GHz) radio flux density versus the γ-ray luminosity calculated using the integrated fluxes estimated in this work. The 5 GHz radio flux densities were taken from the NASA/IPAC Extragalactic Database (NED) except for those objects with references listed below†. We find a strong positive correlation between radio core power at 5GHz and γ-ray luminosity. The right panel shows the radio core dominance parameter versus the γ-ray luminosity calculated using the integrated fluxes estimated in this work. We find no correlation between the radio core dominance parameter of these radio galaxies versus their γ-ray luminosity. The TeV-detected radio galaxies are annotated and highlighted using blue star markers, and we see no clustering of these particular sources. †Fornax A and IC 1531 (Ekers et al. 1989), NGC 1218 (Saikia et al. 1986), NGC 2892 (Kharb & Shastri 2004) and NGC 6251 (Evans et al. 2005).

γ-ray emission from these objects and would render the detection of any spectral break with a non-jet origin difficult, if not impossible.

With the advent of new large observatories such as SKA and CTA, a new era of astronomy is upon us that can help to better understand the non-thermal astroparticle physics at play in AGN-like radio galaxies. Many open questions still remain, such as where and how γ-rays are produced in these extragalactic objects and why a fraction of these largest and most energetically connected objects seen in our universe produce TeV γ-rays despite having much lower Doppler boosting factors compared to blazars? Although we may not get a complete understanding of how these objects work, new discoveries and findings may help to further our knowledge of the characteristics that distinguish between classes of objects under unification schemes, for example multi-wavelength studies across the broad electromagnetic spectrum from low frequency radio observations through to very-high-energy γ-ray observations may provide further support that these unifying characteristics are really down to differences in the masses of their supermassive black holes and their spins, their accretion rates, and the angles and distances at which we view these fascinating objects.

ACKNOWLEDGEMENTS

The authors would like to acknowledge the excellent data and analysis tools provided by the NASA *Fermi*-LAT collaboration, without which this work could not be done. This research has made use of the CTA instrument response functions provided by the CTA Consortium and Observatory; see http://www.cta-observatory.org/science/cta-performance/ (version prod3b-v2) for more details. In addition, this research has made use of the NASA/IPAC Extragalactic Database (NED) which is operated by the Jet Propulsion Laboratory, California Institute of Technology, under contract with the National Aeronautics and Space Administration. This research has also made use of the SIMBAD database, operated at CDS, Strasbourg, France.

Finally, the authors acknowledge the financial support of the UK Science and Technology Facilities Council consolidated grant ST/P000541/1.

REFERENCES

Abdo A. A., et al., 2010, ApJ, 720, 912
Ait Benkhali F., Chakraborty N., Rieger F. M., 2019, A&A, 623, A2
Aleksić J., et al., 2014, Science, 346, 1080
Angioni R., Grandi P., Torresi E., Vignali C., Knödlseder J., 2017, Astroparticle Physics, 92, 42
Angioni R., et al., 2019, A&A, 627, A148
Atwood W. B., et al., 2009, ApJ, 697, 1071
Brown A. M., Adams J., 2011, MNRAS, 413, 2785
Brown A. M., Bœhm C., Graham J., Lacroix T., Chadwick P., Silk J., 2017, Phys. Rev. D, 95, 063018
CTA Consortium Ong R. A., 2019, in European Physical Journal Web of Conferences. p. 01038 (arXiv:1904.12196), doi:10.1051/epjconf/201920901038

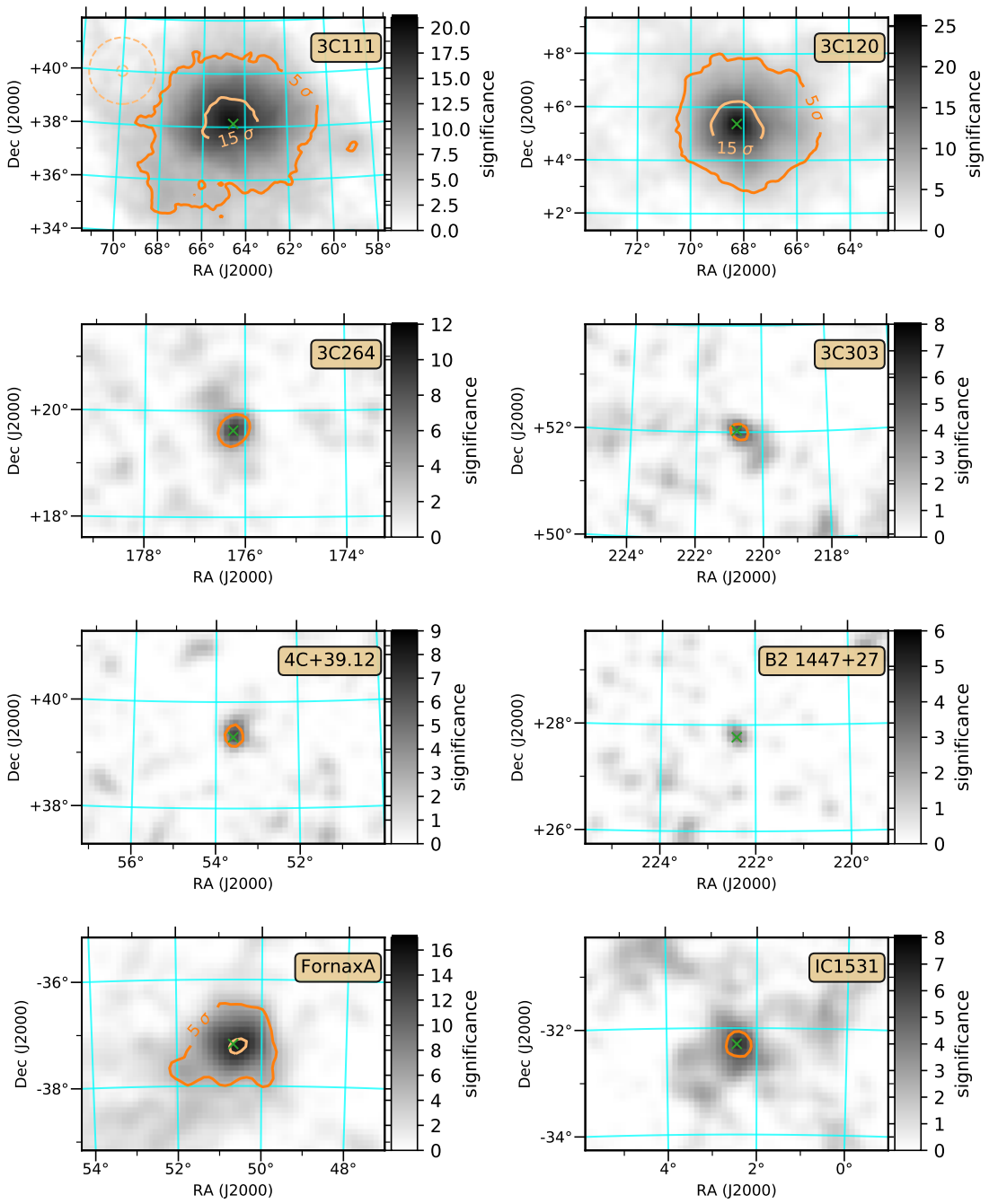

Figure 7. Skymaps showing the significance $\sqrt{\mathrm{TS}}$ for a subset of the radio galaxies analysed. Each skymap considers all energies between 100 MeV $\leq$ E $\leq$ 300 GeV and the intensity scale in the z-axis highlights the significance. The dark-orange solid contour line indicates the 5σ significance boundary and the light-orange solid contour the 15σ significance boundary. The radio galaxy position is indicated with a green $\times$ and the two orange dashed-line concentric circles in the upper left corner of the top left panel show the approximate *Fermi*-LAT PSF at 100 MeV (large) and 1 GeV (small) respectively.

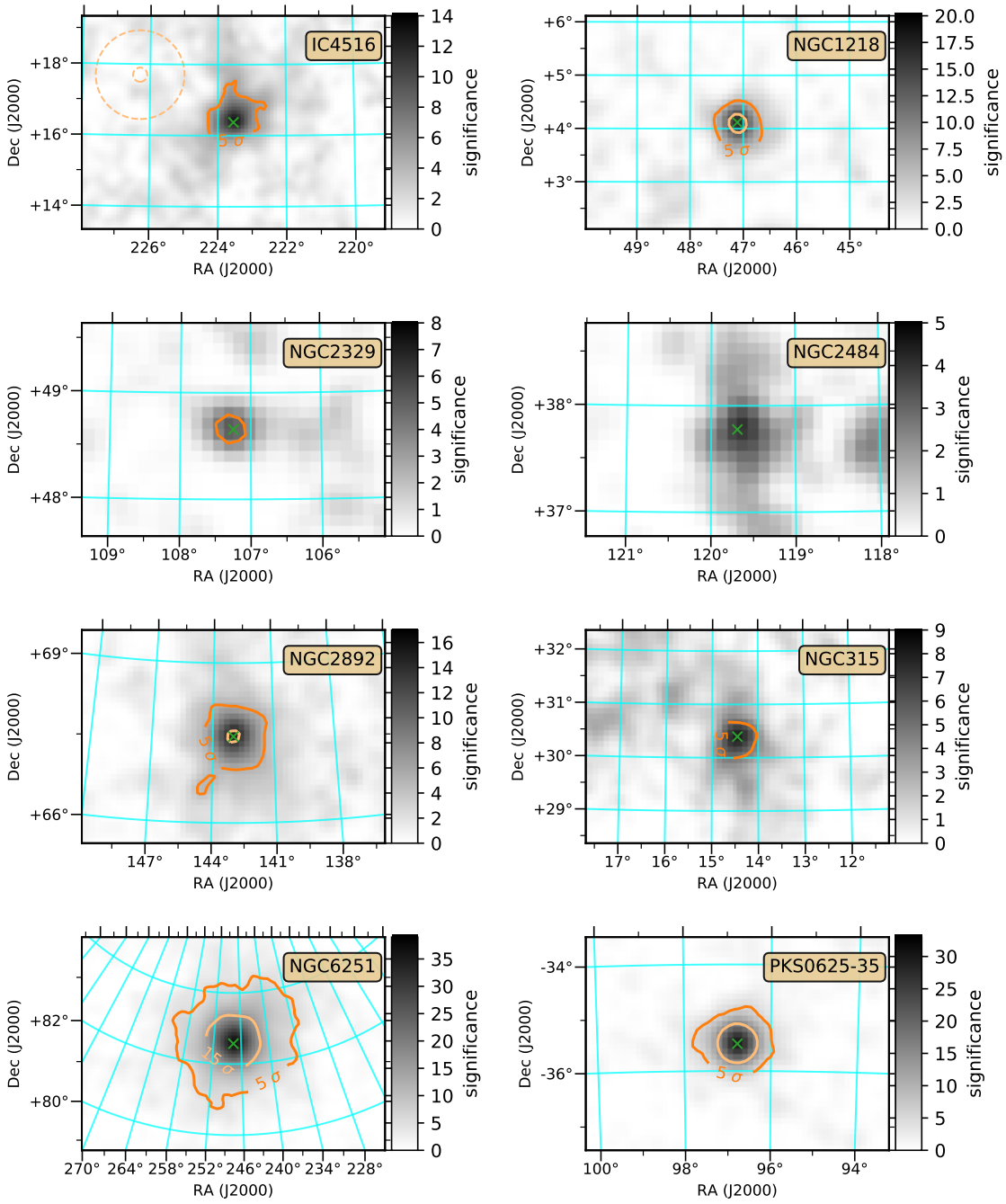

Figure 8. Skymaps showing the significance $\sqrt{\mathrm{TS}}$ for a subset of the radio galaxies analysed. Each skymap considers all energies between 100 MeV $\leq$ E $\leq$ 300 GeV and the intensity scale in the z-axis highlights the significance. The dark-orange solid contour line indicates the 5σ significance boundary and the light-orange solid contour the 15σ significance boundary. The radio galaxy position is indicated with a green $\times$ and the two orange dashed-line concentric circles in the upper left corner of the top left panel show the approximate *Fermi*-LAT PSF at 100 MeV (large) and 1 GeV (small) respectively.

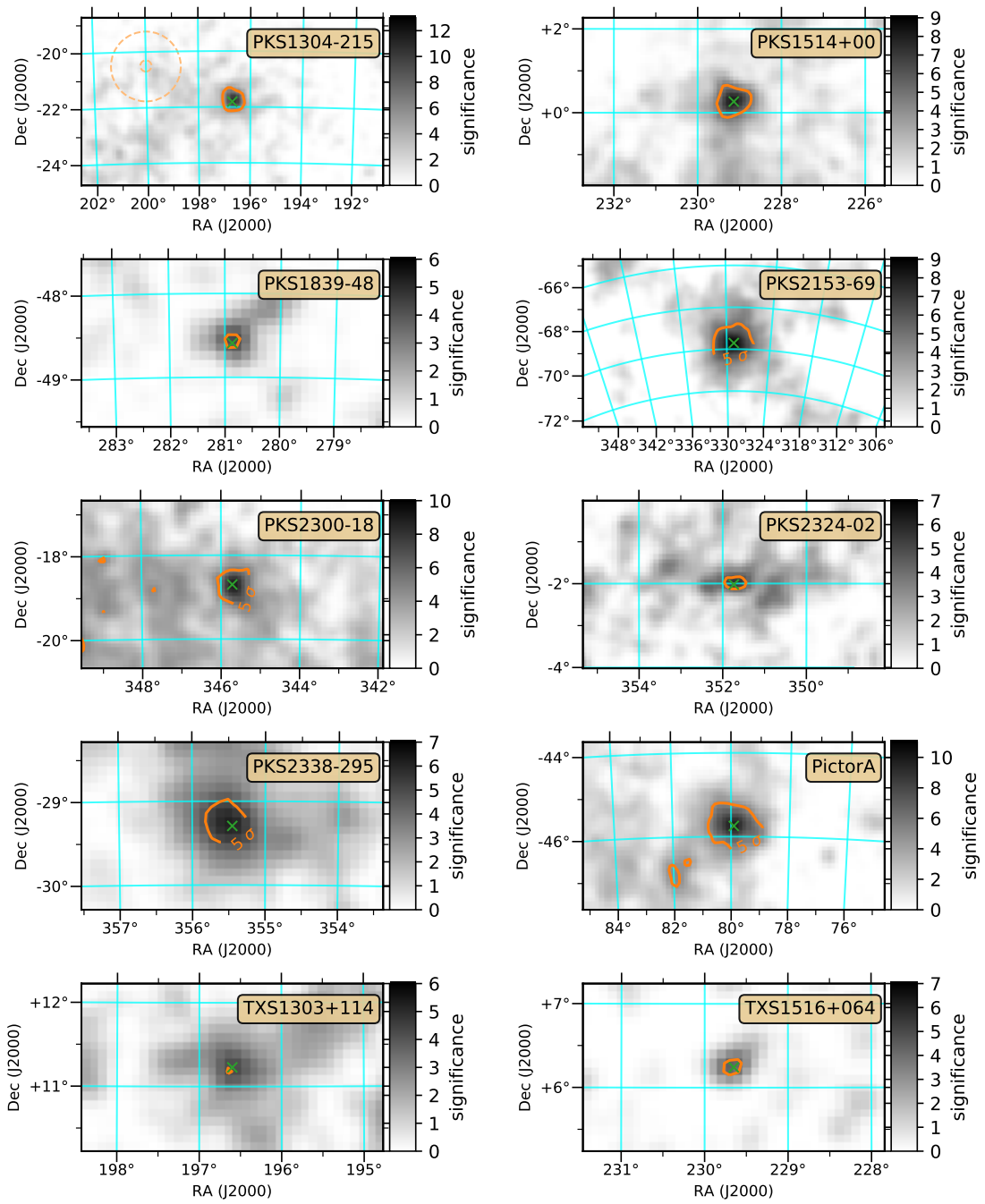

Figure 9. Skymaps showing the significance $\sqrt{\mathrm{TS}}$ for a subset of the radio galaxies analysed. Each skymap considers all energies between 100 MeV $\leq$ E $\leq$ 300 GeV and the intensity scale in the z-axis highlights the significance. The dark-orange solid contour line indicates the 5σ significance boundary and the light-orange solid contour the 15σ significance boundary. The radio galaxy position is indicated with a green $\times$ and the two orange dashed-line concentric circles in the upper left corner of the top left panel show the approximate *Fermi*-LAT PSF at 100 MeV (large) and 1 GeV (small) respectively.

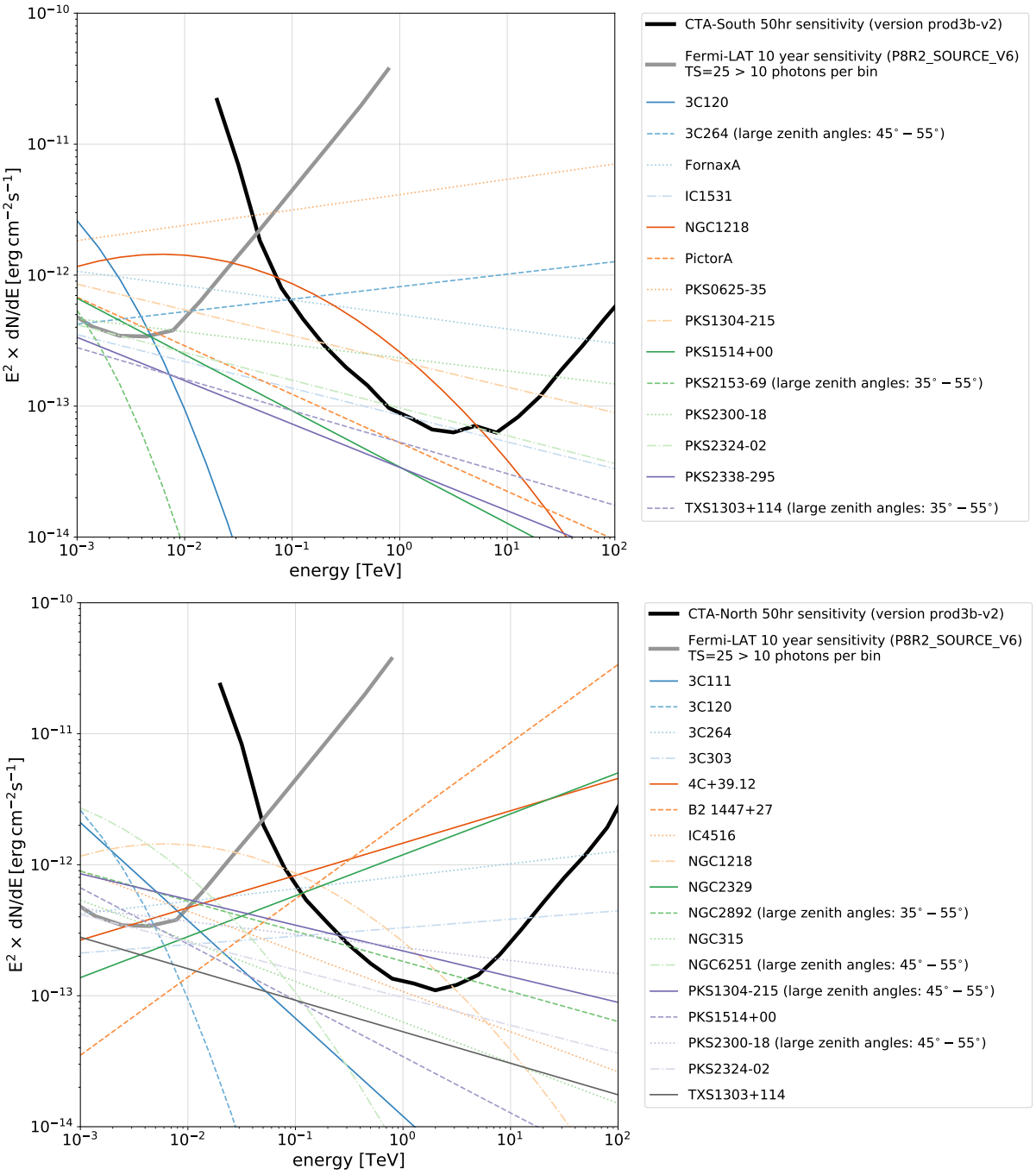

Figure 10. Shown here are the *Fermi*-LAT 4FGL radio galaxy fluxes extrapolated up to 100 TeV for both CTA-South (top panel) and CTA-North (bottom panel). The respective sensitivity performance curves for each of the CTA sites is also shown (solid black line) as well as the *Fermi*-LAT 10 year sensitivity (solid grey line). The *Fermi*-LAT detected fluxes are extrapolated assuming no spectral breaks or features between the GeV and TeV energy range.

Ekers R. D., et al., 1989, Monthly Notices of the Royal Astronomical Society, 236, 737
Evans D. A., Hardcastle M. J., Croston J. H., Worrall D. M., Birkinshaw M., 2005, Monthly Notices of the Royal Astronomical Society, 359, 363
Fan J. H., Zhang J. S., 2003, A&A, 407, 899
Fanaroff B. L., Riley J. M., 1974, MNRAS, 167, 31P
Giannios D., Uzdensky D. A., Begelman M. C., 2009, MNRAS, 395, L29
Graham J. A., Brown A. M., Chadwick P. M., 2019, MNRAS, 485, 3277
H. E. S. S. Collaboration et al., 2018a, MNRAS, 476, 4187
H. E. S. S. Collaboration et al., 2018b, Astronomy and Astrophysics, 619, A71
Hardcastle M. J., Croston J. H., 2011, MNRAS, 415, 133
Kharb P., Shastri P., 2004, Astronomy and Astrophysics, 425, 825
Lacroix T., Bœhm C., Silk J., 2014, Phys. Rev. D, 90, 043508
Massardi M., et al., 2008, Monthly Notices of the Royal Astronomical Society, 384, 775
Mattox J. R., et al., 1996, ApJ, 461, 396

Mukherjee R., 2018, The Astronomer's Telegram, 11436, 1
Nolan P. L., et al., 2012, ApJS, 199, 31
Rieger F. M., 2017, in 6th International Symposium on High Energy Gamma-Ray Astronomy. p. 020008 (arXiv:1611.02986), doi:10.1063/1.4968893
Sahakyan N., Yang R., Aharonian F. A., Rieger F. M., 2013, ApJ, 770, L6
Saikia D. J., Subrahmanya C. R., Patnaik A. R., Unger S. W., Cornwell T. J., Graham D. A., Prabhu T. P., 1986, Monthly Notices of the Royal Astronomical Society, 219, 545
Sanchez D., Holler M., Taylor A., Rieger F., DeNaurois M., for the H.E.S.S. collaboration 2018, in TeVPA. Berlin
Stawarz Ł., Sikora M., Ostrowski M., 2003, ApJ, 597, 186
The Fermi-LAT collaboration 2019, arXiv e-prints, p. arXiv:1902.10045
Urry C. M., Padovani P., 1995, PASP, 107, 803
Wenger M., et al., 2000, Astronomy and Astrophysics Supplement Series, 143, 9
Wood M., Caputo R., Charles E., Di Mauro M., Magill J., Perkins J. S., Fermi-LAT Collaboration 2017, International Cosmic Ray Conference, 301, 824

This paper has been typeset from a TEX/LATEX file prepared by the author.